ACS OMEGA

Article

Cite This: ACS Omega 2018, 3, 6022−6030

Toxic Metal Sequestration Exploiting a Unprecedented Low-Molecular-Weight Hydrogel-to-Metallogel Transformation

Avik De and Raju Mondal*

Department of Inorganic Chemistry, Indian Association for the Cultivation of Science, 2A & 2B Raja S. C. Mullick Road, Jadavpur, Kolkata 700 032, India

Supporting Information

ABSTRACT: We report herein the development of a unique low-molecular-weight gelator-induced technique for environmental remediation. The motive of this work is wastewater purification using a gel-based toxic heavy metal sequestration. The essence of this technique was to bring two different functionalities, one capable of multiple coordination and another with gel-forming ability, arranged in tandem within a single ligand molecule. Naturally, the success of the approach depends on whether the two tandem-arrayed functionalities are indeed working in tandem. Our results show that the ligand molecule is an excellent example of concomitant hydrogelator and metallogelator. The most interesting aspects of this study involve the toxic metal sequestration of Pb, Cd, and Hg which was further studied in detail with spectroscopic, microscopic, and diffraction techniques. We also report here a rare property of pure organic hydrogel-to-metallogel transformation which could open up a new avenue on wastewater purification. In essence, the hydrogels can be envisaged as a unique class of metal-free zeolite analogue for environmental remediation not by just absorbance but through absorbance cum coordination, which are further corroborated by the inductively coupled plasma-optical emission spectroscopy results.

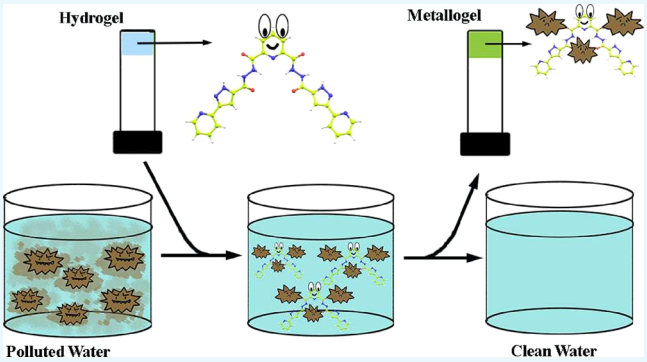

INTRODUCTION

An intriguing correlation between environment and us is that 70% of both human body and earth is made of water.[1,2] Correlation does not imply causation. Notwithstanding, any damage to the most important and ubiquitous ingredient of environment, that is, water, therefore literally can be conceived as a serious self-inflicted body blow for us.[3] Perhaps, that is how Mother Nature restores the balance. Unfortunately, this very balance of the nature has now moved into uncharted waters by our ever increasing lifestyle and subsequent industrial progress.[4,5] However, progress comes at a price; a staggering amount of industrial wastes laden with hazardous toxic metals are dumped in water everyday.[6] Needless to mention, the presence of such contaminated water in the form of three-quarters of our body can wreck havoc.[7,8] Of particular concern is the nonbiodegradable heavy metal ions such as Pb, Cd, or Hg, which can cause serious damage to the central nervous system, kidneys, and immune system of human beings once accumulated beyond a permissible concentration in the body.[9,10] Further corroborations come from some extensively publicized and well-documented massacres caused by water pollution-related diseases such as Minamata or itai-itai.[11,12] Naturally as a preventive measure, removal of such toxic metals from wastewater warrants remediation prior to their disposal in navigable waters or land. A number of techniques for wastewater treatments have been developed over the years including biological treatment, separation, ion-exchange, chemical and electrochemical techniques, and adsorption procedures.[13−27] However, these processes suffer from several disadvantages, such as incomplete removal, high cost including costly regeneration processes, and high energy requirements.[28] Therefore, development of cheaper and more effective methods to treat wastewater has become a matter of utmost importance in contemporary environmental research.[29,30]

Among the other methods, gel-based adsorptions of toxic metals are considerable promise to environmental remediation.[31−39] A popular yet emerging approach includes metallogelation where metal-coordinated network entraps sufficiently large amount of solvent to restrict solid-state aggregation.[40,41] Because of strong coordination bonds, once bound, the metals do not leave their sites under ambient conditions. This should lead to a highly stable toxic metal capturing process with improved wastewater purification. It is noteworthy here that arresting a heavy metal-coordinated network in the gel state especially using low-molecular-weight gelators itself is a formidable task. Needless to say, successful execution of such a task primarily depends on the ligand design.[42−46] Any judicious design of a heavy metal gelator offers a three-pronged

Received: April 19, 2018
Accepted: May 24, 2018
Published: June 4, 2018

DOI: 10.1021/acsomega.8b00758
ACS Omega 2018, 3, 6022−6030

challenge: first, to fit with functional groups containing multiple coordinating sites similar to a typical toxic metal capturing agent; second, the spatial arrangement of functionalities should ensure forming a highly cross-linked, intertwined, three-dimensional network; and finally, to modify the chassis of the ligand particularly the noncoordinating part with functionalities capable of immobilizing a large amount of solvent molecules within the framework, thus fulfilling the most important prerequisite of gelation.[47] In a nutshell, the two-in-one ligand should be a heavy metal capturing agent that also capable of gelation.[48]

In our quest for a cheaper and more efficient gel-based method for environmental remediation, we developed a novel pyridine−pyrazole-based amide molecule, namely, N^2,N^6-bis(5-(3)-(pyridin-2-yl)-1*H*-pyrazole-3(5)-carbonyl)-pyridine-2,6-dicarbohydrazide (BP3D). With the concomitant presence of multiple chelating and solvent immobilizer, functional groups BP3D is deemed to be the best choice for the present study. The two dangling pyridyl−pyrazole moieties of the BP3D molecule alongside a central pyridine ring perfectly suited for metal capturing, whereas converging chelating units at the two ends prevents detrimental coordination polymer formation.[49,50] On the other hand, deliberate introduction of diamide groups in the backbone of BP3D is bound to immobilize a greater amount of solvent molecule, further enhancing the possibility of gel formation. Indeed, a BP3D molecule shows an unprecedented ability to gel toxic heavy metals such as Pb, Cd, and Hg. It is noteworthy here that to the best of our knowledge, a low-molecular-weight gelator-based removal of Pb, Cd, and Hg from wastewater has hitherto not been reported in the literature. We also report here a unique event of supramolecular hydrogel-to-metallohydrogel transformation in the presence of heavy metal salt which has potential applications in gel-based water purification via heavy metal filtering.

RESULTS AND DISCUSSION

The titular gelator, BP3D, can be prepared in high yields by the reaction of 3-(pyridin-2-yl)-1*H*-pyrazole-5-carbohydrazide with 2,6-pyridinedicarbonyl dichloride in a dry acetonitrile medium.

It was abundantly clear that success of our work heavily depends on the spatial orientation of both coordinating and H-bonding functional groups. A two prong pendent orientation of the pyridine−pyrazole moiety would be the most favorable one with enhanced ligand−solvent interaction and a better metal-driven cross-linking network. Naturally, we were interested to know the relative orientation of the functional groups. Fortunately, after numerous attempts, we have been successful in generating diffraction quality single crystals of the ligand from a methanol/dimethylformamide (DMF) solvent system. The crystal structure (monoclinic, *C*2/*c*) (Figure 1a) indeed shows a pendent orientation of the coordinating groups with extensive hydrogen bonding and other intermolecular interactions.[51] The three-dimensional supramolecular self-assembly, on the other hand, is dominated by interlocked $\pi-\pi$ stacking of aromatic rings in a head-to-tail arrangement (Figure 1b).

Although dual purposes for BP3D design involve heavy metal capturing and subsequent metallogelation, it is only prudent to test whether it can form a gel on its own. Indeed, the presence of two bisamide groups makes their mark, and a transparent colorless hydrogel (Figure 2 inset) named here **G-L** was formed at 1 wt % BP3D concentration in the dimethyl sulfoxide (DMSO)/water solvent mixture with the formation of a fibrillar structure, as supported by microscopic data (Figure 2). BP3D is

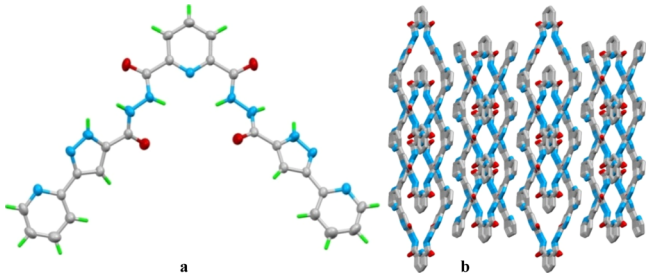

Figure 1. Crystal structure of BP3D showing (a) two prong pendent arrangement of functional groups and (b) supramolecular self-assembly along the *c* axis.

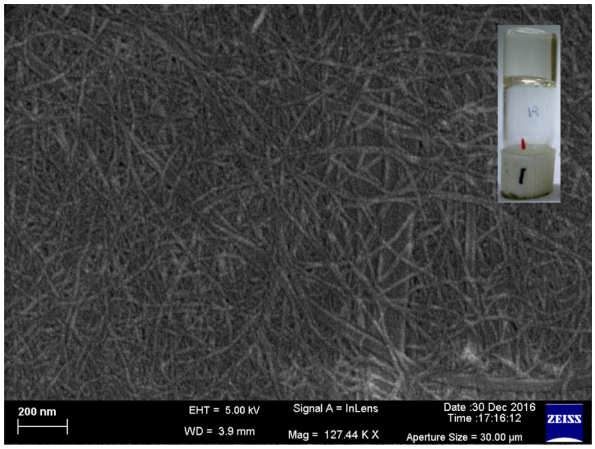

Figure 2. SEM image of hydrogel prepared by 1 wt % BP3D ligand. The inset shows a picture of transparent hydrogel **G-L**.

soluble only in DMF or DMSO. Here, for all of the gelation tests, we have used DMSO as a cosolvent because it is comparatively safer to use. Increasing the wt % makes the gel stronger but makes the gel opaque as well.

Unprecedented Hydrogel-to-Metallohydrogel Transformation. Having confirmed the gelation ability of BP3D, we proceed to the next obvious task that is to find out whether the two tandem-arrayed functionalities targeting multiple coordination and gelation are indeed working in tandem in the presence of a heavy metal. In other words, although solvent immobilizer functionalities are individually actively engaged in supramolecular hydrogel formation, we were interested to see whether concurrent metal coordination of chelating functionalities are also possible in the same gel state. Another point of interest is to check the sustainability of the gel state after metal coordination. It was gratifying to observe that both chelating and gelator functionalities of BP3D are indeed working in tandem and led to a unique event of gel-to-gel transformation or more precisely a postgelation gelator−metal coordination-driven hydrogel-to-metallohydrogel transformation. To assess the role of chelating functionalities in the gel state, aqueous solution of colorless metal salts of lead was added on top of the colorless hydrogel **G-L**. As expected for a routine chemical responsive test, within few minutes, the color of the gel−sol interface turned into yellow, signifying metal complex formation at the upper surface as it came in contact with the metal. Subsequent events, however, were beyond our expectation as the color change does not just stop at the interface but shows an unprecedented downward trend with time. As illustrated in Figure 3a, with time, the *increasing* upper portion

DOI: 10.1021/acsomega.8b00758
ACS Omega 2018, 3, 6022−6030

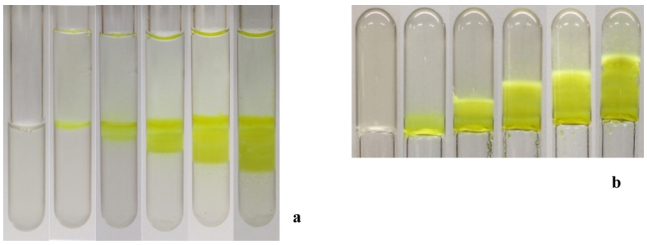

Figure 3. Photographs showing time-dependent hydrogel-to-metallogel transformations, (a) starting from pure hydrogel at the leftmost and subsequent images are taken after one day intervals and (b) same tubes when inverted.

gradually turned into yellow color, whereas the *diminishing* lower portion retained the original colorless state of the mother gel. A tube inversion test further confirms that the yellow colored upper portion is indeed a gel (Figure 3b). Even after the complete transformation of the gel, it was able to hold its weight when the tube was inverted, further reinforcing the notion of gel-to-gel transformation. Similar transformation was also observed for mercury, albeit at a slower pace (Figures S37 and S38). For Cd, no color change was observed; however, distinct change in morphology implies that transformation might have occurred (Figure 4). For transmission electron

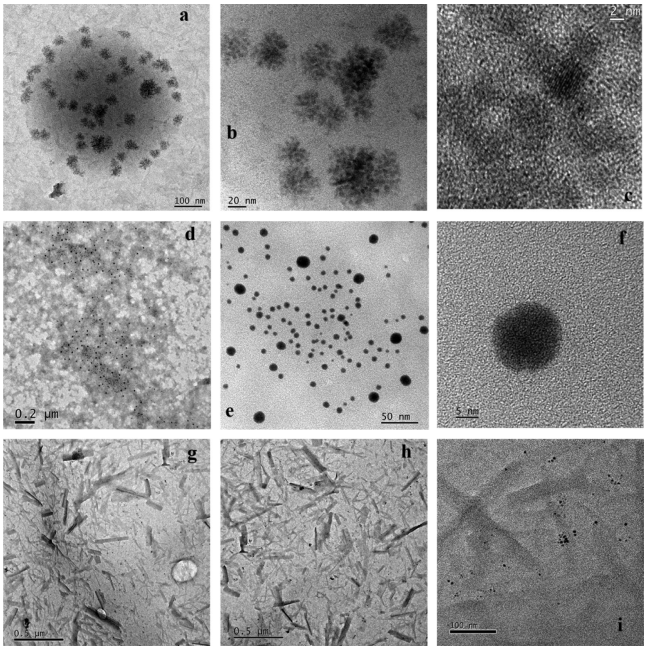

Figure 4. TEM images of transformed metallogel, left to right more zoomed in images. Pb gel (a–c), Hg gel (d–f), and Cd gel (g–i).

microscopy (TEM), we have taken sample from the column of 1 week old column of those transformed metallogel. All of them clearly show the growth of nanoscale metal–organic particles (NMOPs) which start from the fiber. The growth of Pb NMOP is a bit different from other two. For Pb, first, a nanoball of approximate diameter of around 500 nm is formed from fibers in the presence of Pb ion. Then, crystalline NMOPs start to form around it. For Hg and Cd, the NMOP starts to form directly from fibers and also they are noncrystalline (Figure 5). It is noteworthy here that to the best of our knowledge, such kind of hydrogel-to-metallogel transformation in the presence of toxic metal salt solution has hitherto not been reported in the literature.

The obvious questions then arise: does BP3D forms metallogel under normal gelation methods? Are these metallogels identical to those of transformed metallogel? Subsequent experiments give affirmative answers. BP3D does form strong metallogels in the presence of Pb, Cd, and Hg metal salts (named **G-Pb**, **G-Cd**, and **G-Hg**) when standard metallogelation experiments were also carried out separately. Most importantly, comparison of the experimental data confirms that metallogels obtained from the standard method are almost identical to those of the transformed metallogels. However, in order to avoid any confusion, the experimental results of metallogels reported hereafter are those synthesized from standard methods. A general strategy was adopted for standard metallogelation experiments. Aqueous solutions of metal salts were added to a DMSO solution of the ligand, by shaking the sample and leaving it to stand for a few minutes formed stable, opaque/clear metallogels (confirmed by the tube inversion test). A Pb metallogel (**G-Pb**) is formed at a critical gelation concentration of 0.5 wt % after a few minutes of addition of 2 equiv of lead salts. BP3D with $Pb(OAc)_2$ formed the best Pb gel at 1 wt % ligand concentration with 2 equiv of Pb salt in the DMSO/water solvent mixture (ratio DMSO/water = 1:4). Best Hg gel (**G-Hg**) was formed at 1 wt % ligand with 2 equiv of $Hg(OAc)_2$ salt in the DMSO/water solvent mixture (ratio DMSO/water = 2:3). Best Cd gel (**G-Cd**) was formed at 1 wt% ligand with 2 equiv of $Cd(NO_3)_2$ salt in the DMSO/water solvent mixture (ratio DMSO/water = 2:3). **G-Pb** was formed instantly within few second of mixing of ligand and salt solution, but it takes longer time for **G-Hg** and few hours for **G-Cd** to form, though few minutes of sonication makes it much faster. Interestingly, although above gel state could not be achieved from water alone but higher percentage of water facilitates the gel formation. Both hydrogel and metallohydrogels were stable under ambient conditions on a bench top over several weeks (Figure 6).

The formation of gel state can be attributed to supramolecular interactions such as H-bonding and $\pi-\pi$ stacking among solvent and gelator molecules. Comparative Fourier transform infrared (FT-IR) spectroscopy study of ligand and xerogels (Figures S4–S7) was carried out to ascertain the role of diamide and pyridine–pyrazole functional groups in the self-assembly process en route to gelation. In general, decrease in N–H and C═O stretching frequency and increase in N–H bending frequency indicate enhanced intermolecular interactions between amide groups. The ligand, BP3D, shows strong adsorption bands at 3434, 1659, and 1518 cm^{-1} which are due to amide N–H stretching, C═O stretching, and amide N–H bending, respectively. Enhanced intermolecular interactions in the gel state are due to the involvement of C═O and amide N–H group. Decrease in frequency for N–H stretching is a recurring theme as we move on to metallogels, and for Pb, Hg, and Cd xerogels, it appears at 3409, 3412, and 3408 cm^{-1}, respectively. As expected, amide N–H bending frequency, on the other hand, increases to 1528, 1566, and 1519 cm^{-1} for Pb, Hg, and Cd xerogels. For Pb and Cd, the C═O stretching frequency decreases to 1636 and 1605 cm^{-1}; this indicates two possibilities. First, O of C═O coordinated to metal, and second, O is involved in H-bonding formation. On the other hand, C═O stretching frequency remains almost same for Hg at 1661 cm^{-1}. Increasing the value of stretching frequency of C═O indicates that there is a decrease in the extent of H-

DOI: 10.1021/acsomega.8b00758
ACS Omega 2018, 3, 6022–6030

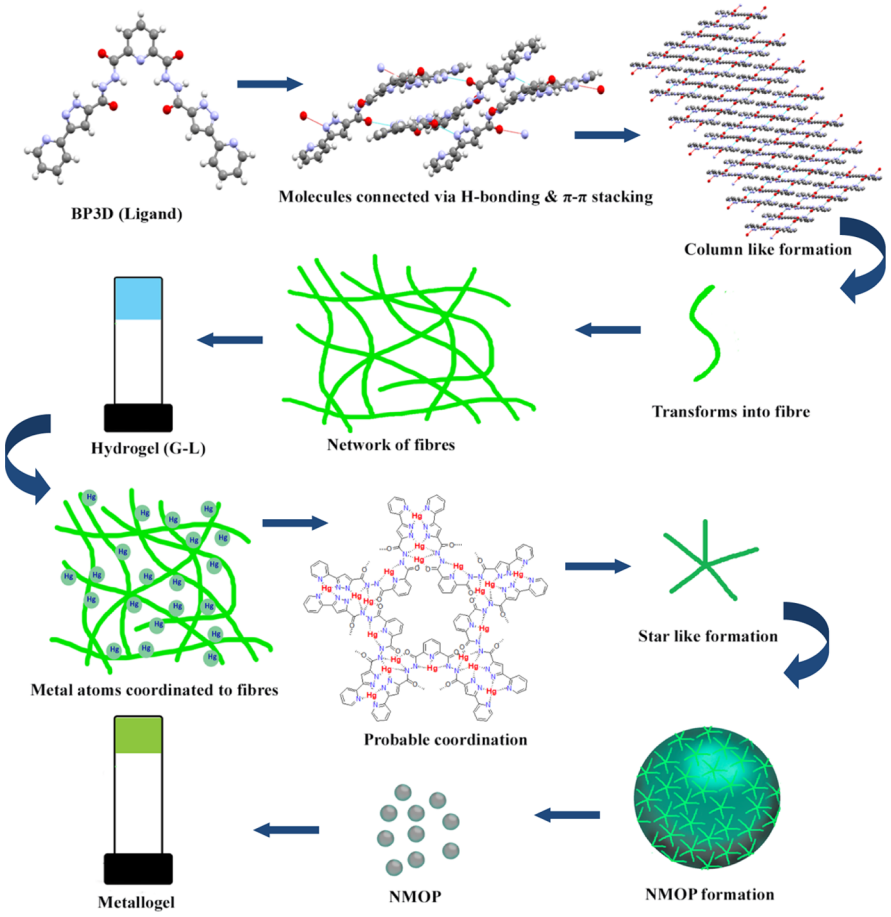

Figure 5. Probable schematic diagram of hydrogel-to-metallogel transformation.

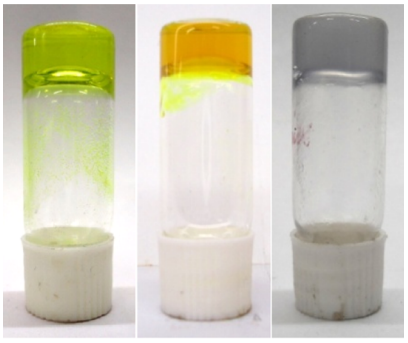

Figure 6. Images of (a) **G-Hg**, (b) **G-Pb**, and (c) **G-Cd** at 1 wt % concentration.

bonding. This is only possible when there is two types of C═O present in the ligand, one of them is participating in H-bonding as well as metal coordination and other is inactive.

G-Pb is much more stronger than **G-Hg** and **G-Cd**, even stronger than **G-L** (Figure 7a). This indicates that stronger ligand−metal coordination bond and more H-bonding are present in **G-Pb** than those in the other metallogels. This is corroborated from the rheology data. All of the rheology experiments were performed with the gels formed at 1 wt % ligand concentration. All four gels are stable up to 10 Pa stress (Figures S26−S29). After that, **G-L**, **G-Hg**, and **G-Cd** start breaking. **G-L** transforms into sol at 27.29 Pa. **G-Hg** and **G-Cd** transform into sol at a bit lower stress value, that is, 25.45 and 18.09 Pa, respectively. **G-Pb** transforms into sol at 153.9 Pa stress. From the rheology data, we can confirm that **G-Pb** is indeed stronger than the **G-Hg** gel. **G-Pb** also shows distinct thixotropic behavior in contrast to others (Figure 7b).

The unusual ability of the BP3D-based hydrogel **G-L** to sequester toxic heavy metals from water via metal−ligand coordination has many implications and was studied in detail using various spectroscopic and microscopic techniques. For example, the UV−vis spectrum of the free ligand and subsequent titration with metal salts with corroborative Job's plots clearly supports the metal−ligand complex formation. UV−vis titration was performed using a 1×10^{-4} M solution of ligand in 1:1 DMSO/water with aliquots of 1×10^{-3} M metal salt solutions. The free ligand shows a strong band at 280 nm which could be assigned to $\pi-\pi^*$ transition. A gradual red shift of this band is a recurrent theme upon sequential addition of metal salts. For Hg, a maximum shift to 298 nm was observed after the addition of 4 equiv for Hg salt. For Pb, the peak is red shifted to around 288 nm with the addition of 2 equiv salts. Subsequent addition of metals does not bring any change to the peak position (Figure 8). For Cd, however, the change in peak positions is not so prominent which suggest that the Cd−BP3D complex is structurally different from Hg and Pb complex (Figure S3). On the other hand, a broad band appears at around 350 nm for Hg and at around 340 nm for Pb which may be due to the intraligand charge transfer. For Cd, also, a very broad band appears at around 345 with increasing intensity.

Further insight in favor of the notion of metal−ligand coordination-driven gel-to-gel transfer comes from the NMR

DOI: 10.1021/acsomega.8b00758
ACS Omega 2018, 3, 6022−6030

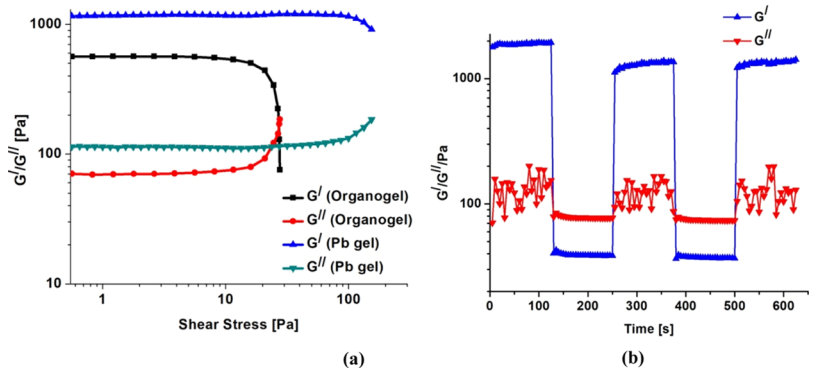

Figure 7. (a) Comparison between stress sweep rheology of hydrogel and **G-Pb** and (b) thixotropic behavior of **G-Pb**.

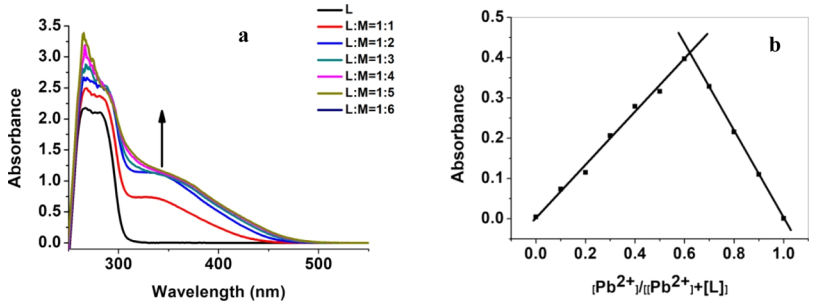

Figure 8. (a) UV titration of BP3DH with Pb at DMSO/water = 1:1 medium and (b) Job's Plot.

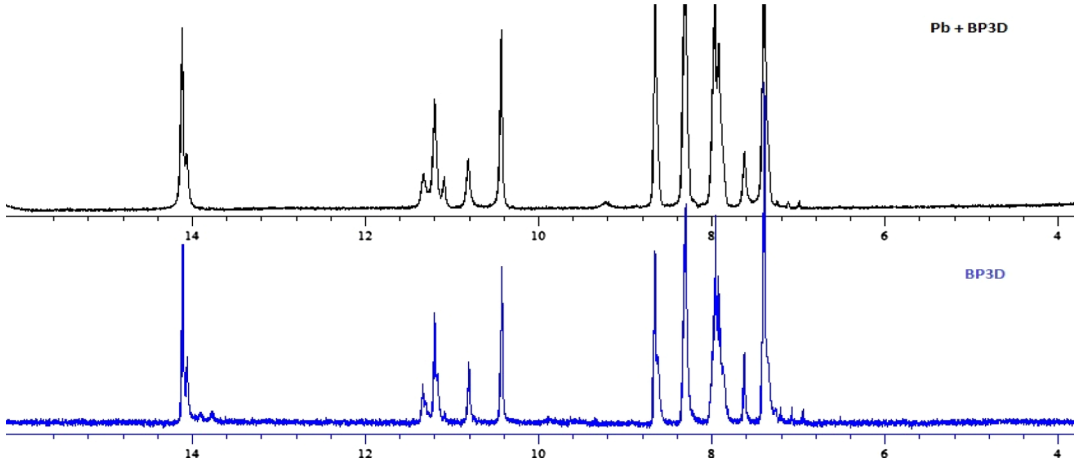

Figure 9. Comparison between ^{1}H NMR spectra of BP3D and Pb metallogel.

spectroscopic studies. A comparative depiction of ^{1}H NMR spectra of metallogels (Figures S10, S12, and S14) compared to that of ligand (Figure S8) is consistent with the literature and shows a common trend of downfield shift and broadening of signals for amide and aromatic protons. The downfield shift and broadening of N−H protons (amide N−H and pyrazole N−H) can be attributed to the extensive H-bonding in the gel state (Figure 9). One the other hand, similar downfieldness features of aromatic protons are characteristic feature of metallogels signifying the interaction between aromatic pi-ring and metals during gelation, while further corroboration comes from the ^{13}C NMR spectra (Figures S9, S11, S13, and S15).

We sought further insight into the microscopic results of **G-L**, **G-Pb**, **G-Hg**, and **G-Cd** to confirm the metallogel produced from the standard procedure is more or less identical to that of transformed metallogels. Detailed morphologies of the gels were studied with field emission scanning electron microscopy (FESEM) and TEM, and atomic force microscopy (AFM) techniques. The scanning electron microscopy (SEM) micrograph of a freshly prepared **G-L** showed the presence of a highly entangled cross-linked fibrillar network with each fibril of infinite length and an average diameter of 20 nm (Figure 2). The individual fibers were found to further assemble to generate bundled aggregates that closely resemble ribbons. In a stark contrast, the metallogels show completely different morphologies. SEM and TEM images of **G-Pb** showed an interesting rhombus-shaped NMOPs of diagonal size of approximately 250 and 300 nm along with fiber-like nature (a diameter of ca. 8 nm) (Figure 10a−c,h,k). The formation of NMOPs was further confirmed by AFM micrographs and energy-dispersive X-ray spectroscopy (EDAX) analysis which was found to contain both the ligand and the metal elements

DOI: 10.1021/acsomega.8b00758
ACS Omega 2018, 3, 6022−6030

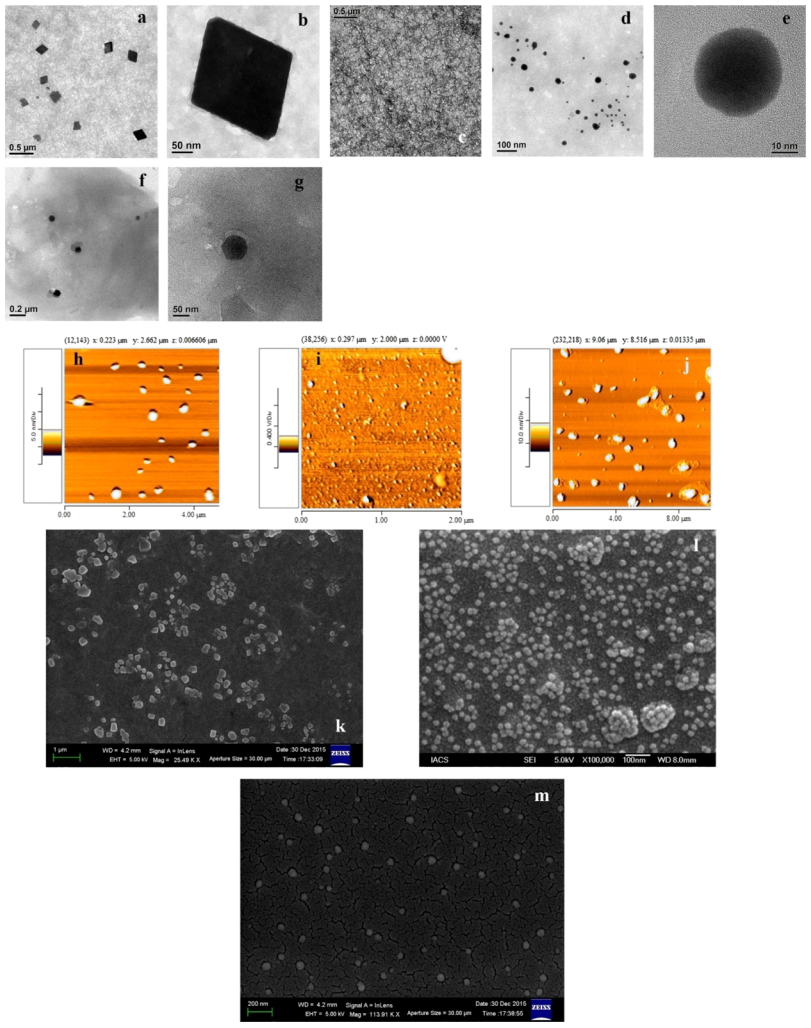

Figure 10. (a–c) TEM images of (a–c) Pb gel, (d,e) Hg gel, and (f,g) Cd gel; AFM images of (h) Pb gel, (i) Hg gel, and (j) Cd gel; and SEM images of (k) Pb gel, (l) Hg gel, and (m) Cd gel.

(Figure S16). On the other hand, appearances of only NMOPs in **G-Hg** (Figure 10d,e,i,l) and **G-Cd** (Figure 10f,g,j,m) vis-à-vis normal fibril network in **G-L** only seems to confirm that this is a dynamic ligand–metal coordination-driven transformation process rather than mere coexistence of two morphologies. For both the metallogels showed no fiber nature, only round-shaped NMOP with an approximate size of 30 nm is visible in the microscopy images. Few particles are even smaller and in the range of 10–20 nm. Interestingly, on the other hand, size of Cd NMOP varies around 70 nm. The selected-area electron diffraction (SAED) patterns of the Hg and Cd NMOPs revealed amorphous nature in comparison to high level of crystallinity in Pb-based NMOPs (Figures S17, S19, and S20).

Toxic Heavy Metal Sequestration. Finally, above singular hydrogel-to-metallohydrogel transformation opens up a new avenue on wastewater purification. In essence, the hydrogel represents a unique class of metal-free zeolite analogue for environmental remediation not by just absorbance but through absorbance cum coordination. The inductively coupled plasma-optical emission spectroscopy (ICP-OES) data of metal concentration taken during above transformation will put this into perspective (Table 1). Experiments were carried out adding metal solutions of known concentration on top of the hydrogel column of 2 mL and 1 wt % concentration. Our intention was to study the possibility of developing a simple but efficient low-cost **G-L** column that could be used as toxic heavy metal sequestration through mere filtering. Subsequently, the aliquots were taken from time to time and measured for metal concentrations. The transformation rate for Cd was really slow, and subsequent changes in concentrations were insignificant. On the other hand, concentration of Pb shows a downward trend from an initial 301.5 to 205.1 mg/L after 15 days to an impressive 43.34 mg/L (85.63% removal) after 3 months. Similar trend was also observed for Hg with a reduction of concentration from 24.12 to 12.27 mg/L after first 15 days and as low as 0.011 mg/L (99.95% removal) after 3 months. Of course, the loss in metal concentration on the upper solution layer was the gain in the lower gel state as evident from a distinctive color change. As illustrated in Figure 3a, with time as the transformation brings about a gradual change of color of the

Table 1. Removal of Toxic Metals

metal	initial amount in aliquot (mg/L)	amt. present after 15 days in aliquot (mg/L)	amt. present after 3 month in aliquot (mg/L)	removal % after 3 month
Pb	301.5	205.1	43.34	85.63
Hg	24.12	12.27	0.011	99.95

DOI: 10.1021/acsomega.8b00758
ACS Omega 2018, 3, 6022–6030

column from colorless to bright yellow. The lower concentration of metal simply means lower amount of toxic metals in the residual water and thus vindicate our plan of using hydrogel column for water purification.

CONCLUSIONS

As a part of our quest on environmental remediation, we have developed a unique gel-based toxic heavy metal sequestration technique. The task was achieved with the design of a two-in-one ligand molecule combining the basic characteristics of a heavy metal capturing agent and low-molecular-weight gelator molecule. The motive was wastewater purification through heavy metal gelation. Accordingly, a pyridine−pyrazole-based two prong pendent ligand (BP3D) fitted with multiple number of coordinating sites for heavy metal capturing, and two diamide arms for gelation were synthesized and utilized. Both functional groups work in tandem and show an unusual gelation of toxic heavy metals such as Pb, Cd, and Hg. Interestingly, above metallogelation of toxic metals can also be achieved via an unprecedented metal−ligand coordination-driven hydrogel-to-metallohydrogel transformation. To the best of our knowledge, such kind of transformation hitherto has not been reported in the literature but has a huge potential application in gel-based wastewater purification simply by using hydrogel column as a filter. We are currently working on improving the efficiency and the rate of toxic metal removal which will be communicated in our future endeavor.

EXPERIMENTAL SECTION

Materials. All reagent grade materials and organic solvents were purchased from Sigma-Aldrich, Alfa Aesar, and Merck and used without further purification. Double distilled water was used for all experiments except in the case of ICP-OES experiment where Milli-Q water was used.

General Experiments. *Hydrogel (**G-L**) Formation.* In a 5 mL vial, BP3D (10 mg, 0.019 mmol) was dissolved into 0.5 mL of DMSO. H_2O (0.5 mL) was added to it under stirring. It was sonicated for few minutes to form a transparent colorless hydrogel.

*Pb Metallohydrogel (**G-Pb**) Formation.* In a 5 mL vial, BP3D (10 mg, 0.019 mmol) was dissolved into 0.2 mL of DMSO. An aqueous solution of $Pb(OAc)_2$ (14 mg, 0.037 mmol in 0.8 mL H_2O) was added to it under stirring. Solution turns yellow color and transforms into strong gel after few seconds.

*Hg Metallohydrogel (**G-Hg**) Formation.* In a 5 mL vial, BP3D (10 mg, 0.019 mmol) was dissolved into 0.4 mL of DMSO. An aqueous solution of $Hg(OAc)_2$ (11.84 mg, 0.037 mmol in 0.6 mL H_2O) was added to it under stirring. Solution turns greenish yellow color. It was sonicated for few minutes and transforms into gel.

*Cd Metallohydrogel (**G-Cd**) Formation.* In a 5 mL vial, BP3D (10 mg, 0.019 mmol) was dissolved into 0.4 mL of DMSO. An aqueous solution of $Cd(NO_3)_2$ (8.79 mg, 0.037 mmol in 0.6 mL H_2O) was added to it under stirring. It was sonicated for few minutes and transforms into colorless gel.

NMR Spectroscopy. ^1H and ^{13}C NMR spectra were recorded on Bruker spectrometers operating at 400 and 500 MHz dissolving the compounds in the DMSO-d_6 solvent. The chemical shift data are reported in units of δ (ppm) relative to tetramethylsilane and referenced with residual DMSO.

X-ray Crystallography. X-ray diffraction intensities for the BP3D crystal was collected at room temperature on Bruker APEX-2 CCD and diffractometer using Mo Kα radiation and processed using SAINT. The structures were solved by direct methods in SHELXS and refined by full-matrix least squares on F2 in SHELXL.[52] We are unable to exactly locate H-atoms attached with N4 and therefore omitted in the CIF file. Crystallographic data are summarized in ref 51, and CIF files for the structures reported in this paper have been deposited with the Cambridge Crystallographic Data Centre (CCDC). Deposition numbers are given in ref 51. Powder X-ray Diffraction (PXRD) patterns were collected at ambient temperature using a Bruker AXS D8 ADVANCE diffractometer.

Scanning Electron Microscopy. A small amount of sample was placed on a clean glass slide and then dried by slow evaporation. The material was then allowed to dry under vacuum at 30 °C for 2 days. The materials were silver-coated, and the micrographs were taken in FESEM apparatus Jeol Scanning Microscope-JSM-6700F and Carl Zeiss AG SUPRA 55 VP-41-32.

Transmission Electron Microscopy. A small amount of sample was placed in a glass vial. Ethanol (1 mL) was added to it, and the vial was sonicated for few hours. Then, 1 drop of this solution was drop casted on a 300 mesh carbon-coated copper grid, and it was mounted on a Jeol JEM 2010 HRTEM.

Rheology. Rheological measurements were taken on an Anton Paar MCR 102 Rheometer with a 25 mm parallel plate. The gap was fixed at 300 μm. A gel sample was preformed in a 5 mL vial and transferred onto the Peltier plate. All measurements were performed at 25 °C. The stress sweep study was performed with a stress ramp from 0.1 to 200 Pa at an angular frequency of 6.284 rad/s. The thixotropic experiment with **G-Pb** was carried out using a five-step process. Here, we determine change of storage modulus (G') and loss (G'') modulus with respect to time. First, when 0.05% strain is applied, it shows its gel property. Then, when 30% strain is applied, it transforms into sol. When we remove the higher strain, it goes back to gel state. Same cycle was repeated for one more time.

Inductively Coupled Plasma-Optical Emission Spectroscopy. ICP-OES measurements were taken on a PerkinElmer Optima 2100 DV. Mercury Standard for ICP was used for the generation of calibration curve before the measurement of the amount of mercury in the aliquot. Multielement standard for ICP was used for generation of calibration curve before the measurement of the amount of Pb and Cd separately.

Other Experimental Methods. FT-IR spectra were performed on a Nicolet MAGNA-IR 750 spectrometer with the KBr pellets containing the samples. UV−visible studies were performed in a PerkinElmer Lambda 950 UV−vis instrument. The elemental analyses were carried out using a PerkinElmer 2400 Series-II CHN analyzer.

Synthetic Procedure. *Synthesis of BP3DH.* BP3D was prepared by the reaction of 3-(pyridin-2-yl)-1*H*-pyrazole-5-carbohydrazide with 2,6-pyridinedicarbonyl dichloride. 2,6-Pyridinedicarbonyl dichloride (2.04 g, 10 mmol) was dissolved in dry acetonitrile and to it 3-(pyridin-2-yl)-1*H*-pyrazole-5-carbohydrazide (10.75 g, 20 mmol) was added, giving an immediate white suspension. The reaction mixture was refluxed overnight at 80 °C, cooled, and filtered. The precipitate was washed with acetonitrile and dried in vacuum. To the suspension of the hydrochloride salt in water, was added saturated sodium bicarbonate solution till slightly basic and stirred at room temperature overnight. The precipitated solid

DOI: 10.1021/acsomega.8b00758
ACS Omega 2018, 3, 6022−6030

was filtered, washed with water, dried, and purified from DMF/water. Yield 50% obtained. Elem. Anal. for $C_{25}H_{19}N_{11}O_4$ calcd: C, 55.86; H, 3.56; N, 28.67; O, 11.91. Found: C, 55.69; H, 3.33; N, 28.89; O, 12.32, ^{1}H NMR spectra/δ (ppm) (500 MHz, DMSO-d_6): 14.113 (s, 2H, pz NH), 11.208 (d, 2H, amide NH), 10.428 (d, 2H, amide NH), 8.658 (d, 2H, pyH), 8.304 (m, 3H, aromatic H), 7.961 (m, 4H, aromatic H), 7.629 (s, 2H, pzH), 7.416 (d, 2H, pyH), IR (KBr, cm^{-1}): 3443 (br), 3223 (br) 1659 (s), 1519 (m).

■ ASSOCIATED CONTENT

Supporting Information

The Supporting Information is available free of charge on the ACS Publications website at DOI: 10.1021/acsomega.8b00758.

Synthetic procedure, UV−vis titration data, IR spectra, NMR spectra, SAED, and EDAX data collected from HR-TEM, AFM images, PXRD data, rheological data, representative procedure for ICP-OES samples, images of different gelation study, images depicting thixotropic property of Pb gel, and images of chemical responsiveness of hydrogel with Hg salt solution (PDF)

Crystallographic data of SHELXS (CIF)

Accession Codes

CCDC 1575681 contains the supplementary crystallographic data for this paper. These data can be obtained free of charge via www.ccdc.cam.ac.uk/data_request/cif, or by emailing data_request@ccdc.cam.ac.uk, or by contacting The Cambridge Crystallographic Data Centre, 12 Union Road, Cambridge CB2 1EZ, UK; fax: +44 1223 336033.

■ AUTHOR INFORMATION

Corresponding Author

*E-mail: icrm@iacs.res.in. Phone: +91 33 24734971. Fax: +91 33 24732805 (R.M.).

ORCID

Avik De: 0000-0003-4127-1555

Raju Mondal: 0000-0002-9013-7259

Notes

The authors declare no competing financial interest.

■ ACKNOWLEDGMENTS

R.M. gratefully acknowledges Science and Engineering research Board (SERB) (project no. SB/EMEQ-301/2014) India, for financial assistance. A.D. thanks DST India for a INSPIRE fellowship. We thank Samirul Islam, Dept. of Materials Science, Indian Association for the Cultivation of Science, for his assistance in collecting ICP-OES data.

■ ABBREVIATIONS

BP3D, N^2,N^6-bis(5(3)-(pyridin-2-yl)-1*H*-pyrazole-3(5)-carbonyl)-pyridine-2,6-dicarbohydrazide; ICP-OES, inductively coupled plasma optical emission spectrometry

■ REFERENCES

(1) Guyton, A. C. *Textbook of Medical Physiology*, 5th ed.; Saunders: Philadelphia, 1976; p xxxvi, 1194 p.

(2) Jackson, S. M.; Lane, S. *Personal and Community Health*; Bailliere Tindall: London, 1975; p viii, 216, 8 p.

(3) Lovett, G. M.; Tear, T. H.; Evers, D. C.; Findlay, S. E. G.; Cosby, B. J.; Dunscomb, J. K.; Driscoll, C. T.; Weathers, K. C. Effects of air pollution on ecosystems and biological diversity in the eastern United States. *Ann. N.Y. Acad. Sci.* **2009**, *1162*, 99−135.

(4) Rosen, A. A. Chemists discuss water resource management - 1. Chemistry of water pollution control: discovering the source and scope of chemical pollution. *Environ. Sci. Technol.* **1967**, *1*, 297−298.

(5) Zimmerman, J. B.; Mihelcic, J. R.; Smith, J. Global Stressors on Water Quality and Quantity. *Environ. Sci. Technol.* **2008**, *42*, 4247−4254.

(6) Dean, R. B. Ultimate disposal of waste water concentrates to the environment. *Environ. Sci. Technol.* **1968**, *2*, 1079−1086.

(7) Duruibe, J.; Ogwuegbu, M.; Egwurugwu, J. Heavy metal pollution and human biotoxic effects. *Int. J. Phys. Sci.* **2007**, *2*, 112−118.

(8) Montgomery, M. A.; Elimelech, M. Water And Sanitation in Developing Countries: Including Health in the Equation. *Environ. Sci. Technol.* **2007**, *41*, 17−24.

(9) Jarup, L. Hazards of heavy metal contamination. *Br. Med. Bull.* **2003**, *68*, 167−182.

(10) Mance, G. *Pollution Threat of Heavy Metals in Aquatic Environments*; Elsevier Applied Science; Sole Distributor in the USA and Canada Elsevier Science: London, 1987; p xii, 372 p.

(11) Balogh, S. J.; Tsui, M. T.-K.; Blum, J. D.; Matsuyama, A.; Woerndle, G. E.; Yano, S.; Tada, A. Tracking the fate of mercury in the fish and bottom sediments of Minamata Bay, Japan, using stable mercury isotopes. *Environ. Sci. Technol.* **2015**, *49*, 5399−5406.

(12) Grossman, E. A.; Freeman, C. S. Estimation of Risk of Kidney Dysfunction from Exposure to Cadmium Using Studies of Occupationally Exposed Workers. In *Environmental Epidemiology*; Draper, W. M., Eds.; American Chemical Society, 1994; Vol. *241*, pp 175−187.

(13) Aziz, H. A.; Adlan, M. N.; Ariffin, K. S. Heavy metals (Cd, Pb, Zn, Ni, Cu and Cr(III)) removal from water in Malaysia: post treatment by high quality limestone. *Bioresour. Technol.* **2008**, *99*, 1578−1583.

(14) Barakat, M. A. Adsorption of Heavy Metals from Aqueous Solutions on Synthetic Zeolite. *Res. J. Environ. Sci.* **2008**, *2*, 13−22.

(15) Blöcher, C.; Dorda, J.; Mavrov, V.; Chmiel, H.; Lazaridis, N. K.; Matis, K. A. Hybrid flotation−membrane filtration process for the removal of heavy metal ions from wastewater. *Water Res.* **2003**, *37*, 4018−4026.

(16) Dean, J. G.; Bosqui, F. L.; Lanouette, K. H. Removing heavy metals from waste water. *Environ. Sci. Technol.* **1972**, *6*, 518−522.

(17) Fu, F.; Wang, Q. Removal of heavy metal ions from wastewaters: A review. *J. Environ. Manage.* **2011**, *92*, 407−418.

(18) Shen, Z.; Wu, D.; Yang, J.; Yuan, T.; Wang, W.; Jia, J. Methods to improve electrochemical treatment effect of dye wastewater. *J. Hazard. Mater.* **2006**, *131*, 90−97.

(19) Tripathi, P. K.; Liu, M.; Zhao, Y.; Ma, X.; Gan, L.; Noonan, O.; Yu, C. Enlargement of uniform micropores in hierarchically ordered micro-mesoporous carbon for high level decontamination of bisphenol A. *J. Mater. Chem. A* **2014**, *2*, 8534−8544.

(20) Crittenden, J. C. *Montgomery Watson Harza (Firm), Water Treatment Principles and Design*, 2nd ed.; John Wiley & Sons: Hoboken, NJ, 2005; p xx, 1948 p.

(21) Liang, H.-W.; Cao, X.; Zhang, W.-J.; Lin, H.-T.; Zhou, F.; Chen, L.-F.; Yu, S.-H. Robust and Highly Efficient Free-Standing Carbonaceous Nanofiber Membranes for Water Purification. *Adv. Funct. Mater.* **2011**, *21*, 3851−3858.

(22) Shannon, M. A.; Bohn, P. W.; Elimelech, M.; Georgiadis, J. G.; Mariñas, B. J.; Mayes, A. M. Science and technology for water purification in the coming decades. *Nature* **2008**, *452*, 301−310.

(23) Sun, M.-H.; Huang, S.-Z.; Chen, L.-H.; Li, Y.; Yang, X.-Y.; Yuan, Z.-Y.; Su, B.-L. Applications of hierarchically structured porous materials from energy storage and conversion, catalysis, photocatalysis, adsorption, separation, and sensing to biomedicine. *Chem. Soc. Rev.* **2016**, *45*, 3479−3563.

(24) Sun, Q.; Aguila, B.; Perman, J.; Earl, L. D.; Abney, C. W.; Cheng, Y.; Wei, H.; Nguyen, N.; Wojtas, L.; Ma, S. Postsynthetically Modified Covalent Organic Frameworks for Efficient and Effective Mercury Removal. *J. Am. Chem. Soc.* **2017**, *139*, 2786−2793.

(25) Veliscek-Carolan, J.; Jolliffe, K. A.; Hanley, T. L. Effective Am(iii)/Eu(iii) separations using 2,6-bis(1,2,4-triazin-3-yl)pyridine

DOI: 10.1021/acsomega.8b00758
ACS Omega 2018, 3, 6022−6030

(BTP) functionalised titania particles and hierarchically porous beads. *Chem. Commun.* **2015**, *51*, 11433−11436.
(26) Yang, X.-Y.; Chen, L.-H.; Li, Y.; Rooke, J. C.; Sanchez, C.; Su, B.-L. Hierarchically porous materials: synthesis strategies and structure design. *Chem. Soc. Rev.* **2017**, *46*, 481−558.
(27) Zhu, Y.-P.; Liu, Y.-L.; Ren, T.-Z.; Yuan, Z.-Y. Hollow manganese phosphonate microspheres with hierarchical porosity for efficient adsorption and separation. *Nanoscale* **2014**, *6*, 6627−6636.
(28) Eccles, H. Treatment of metal-contaminated wastes: why select a biological process? *Trends Biotechnol.* **1999**, *17*, 462−465.
(29) Babel, S.; Kurniawan, T. A. Low-cost adsorbents for heavy metals uptake from contaminated water: a review. *J. Hazard. Mater.* **2003**, *97*, 219−243.
(30) Barakat, M. A. New trends in removing heavy metals from industrial wastewater. *Arabian J. Chem.* **2011**, *4*, 361−377.
(31) Çavuş, S.; Gürdağ, G.; Sözgen, K.; Gürkaynak, M. A. The preparation and characterization of poly(acrylic acid-co-methacrylamide) gel and its use in the non-competitive heavy metal removal. *Polym. Adv. Technol.* **2009**, *20*, 165−172.
(32) Ju, X.-J.; Zhang, S.-B.; Zhou, M.-Y.; Xie, R.; Yang, L.; Chu, L.-Y. Novel heavy-metal adsorption material: ion-recognition P(NIPAM-co-BCAm) hydrogels for removal of lead(II) ions. *J. Hazard. Mater.* **2009**, *167*, 114−118.
(33) Knerr, P. J.; Branco, M. C.; Nagarkar, R.; Pochan, D. J.; Schneider, J. P. Heavy metal ion hydrogelation of a self-assembling peptideviacysteinyl chelation. *J. Mater. Chem.* **2012**, *22*, 1352−1357.
(34) Okesola, B. O.; Smith, D. K. Applying low-molecular weight supramolecular gelators in an environmental setting - self-assembled gels as smart materials for pollutant removal. *Chem. Soc. Rev.* **2016**, *45*, 4226−4251.
(35) Özkahraman, B.; Acar, I.; Emik, S. Removal of Cu2+ and Pb2+ Ions Using CMC Based Thermoresponsive Nanocomposite Hydrogel. *Clean: Soil, Air, Water* **2011**, *39*, 658−664.
(36) Paulino, A. T.; Belfiore, L. A.; Kubota, L. T.; Muniz, E. C.; Tambourgi, E. B. Efficiency of hydrogels based on natural polysaccharides in the removal of Cd2+ ions from aqueous solutions. *Chem. Eng. J.* **2011**, *168*, 68−76.
(37) Yang, S.; Fu, S.; Liu, H.; Zhou, Y.; Li, X. Hydrogel beads based on carboxymethyl cellulose for removal heavy metal ions. *J. Appl. Polym. Sci.* **2011**, *119*, 1204−1210.
(38) Dave, N.; Chan, M. Y.; Huang, P.-J. J.; Smith, B. D.; Liu, J. Regenerable DNA-Functionalized Hydrogels for Ultrasensitive, Instrument-Free Mercury(II) Detection and Removal in Water. *J. Am. Chem. Soc.* **2010**, *132*, 12668−12673.
(39) Esser-Kahn, A. P.; Iavarone, A. T.; Francis, M. B. Metallothionein-Cross-Linked Hydrogels for the Selective Removal of Heavy Metals from Water. *J. Am. Chem. Soc.* **2008**, *130*, 15820−15822.
(40) Piepenbrock, M.-O. M.; Clarke, N.; Steed, J. W. Metal Ion and Anion-Based "Tuning" of a Supramolecular Metallogel. *Langmuir* **2009**, *25*, 8451−8456.
(41) Tam, A. Y.-Y.; Yam, V. W.-W. Recent advances in metallogels. *Chem. Soc. Rev.* **2013**, *42*, 1540−1567.
(42) Carter, K. K.; Rycenga, H. B.; McNeil, A. J. Improving Hg-Triggered Gelation via Structural Modifications. *Langmuir* **2014**, *30*, 3522−3527.
(43) Ghosh, B. N.; Bhowmik, S.; Mal, P.; Rissanen, K. A highly selective, Hg2+ triggered hydrogelation: modulation of morphology by chemical stimuli. *Chem. Commun.* **2014**, *50*, 734−736.
(44) King, K. N.; McNeil, A. J. Streamlined approach to a new gelator: inspiration from solid-state interactions for a mercury-induced gelation. *Chem. Commun.* **2010**, *46*, 3511−3513.
(45) Sengupta, S.; Mondal, R. A novel gel-based approach to wastewater treatment - unique one-shot solution to potentially toxic metal and dye removal problems. *J. Mater. Chem. A* **2014**, *2*, 16373−16377.
(46) Yadav, P.; Ballabh, A. Room temperature metallogelation for a simple series of aminothiazole ligands with potential applications in identifying and scavenging mercury ions. *RSC Adv.* **2014**, *4*, 563−566.
(47) Bala, S.; Mondal, R. Gel−based Controlled Synthesis of Silver Nanoparticles and Their Applications in Catalysis, Sensing and Environmental Remediation. *ChemistrySelect* **2017**, *2*, 389−398.
(48) Malviya, N.; Das, M.; Mandal, P.; Mukhopadhyay, S. A smart organic gel template as metal cation and inorganic anion sensor. *Soft Matter* **2017**, *13*, 6243.
(49) Bhattacharya, S.; Sengupta, S.; Bala, S.; Goswami, A.; Ganguly, S.; Mondal, R. Pyrazole-Based Metallogels Showing an Unprecedented Colorimetric Ammonia Gas Sensing through Gel-to-Gel Transformation with a Rare Event of Time-Dependent Morphology Transformation. *Cryst. Growth Des.* **2014**, *14*, 2366−2374.
(50) Sengupta, S.; Mondal, R. Elusive Nanoscale Metal−Organic-Particle-Supported Metallogel Formation Using a Nonconventional Chelating Pyridine−Pyrazole-Based Bis-Amide Ligand. *Chem.—Eur. J.* **2013**, *19*, 5537−5541.
(51) Crystallographic data for compound BP3D ($C_{25}H_{19}N_{11}O_4$), CCDC deposition number 1575681, chemical formula weight = 537.51, monoclinic, space group: $C_{2/C}$, a = 20.463(2) Å, b = 8.8637(9) Å, c = 14.0198(14) Å, α = 90.00, β = 111.426(3), γ = 90.00, V = 2367.1(4) Å^3, R1 = 0.0625, wR2 = 0.1691, Z = 4, reflections collected = 15737, unique reflections = 2718, observed reflections [$I > 2\sigma(I)$] = 1369, D = 1.508 g cm^{-3}, μ = 0.109 mm^{-1}.
(52) Sheldrick, G. M. Crystal structure refinement with SHELXL. *Acta Crystallogr., Sect. C: Struct. Chem.* **2015**, *71*, 3−8.

DOI: 10.1021/acsomega.8b00758
ACS Omega 2018, 3, 6022−6030